International Journal of Nanomedicine

Dovepress
open access to scientific and medical research

Open Access Full Text Article

ORIGINAL RESEARCH

Smart Fe_3O_4@ZnO Core-Shell Nanophotosensitizers Potential for Combined Chemo and Photodynamic Skin Cancer Therapy Controlled by UVA Radiation

Qian Ren[1], Caixia Yi[2], Jun Pan[1], Xin Sun[2], Xiao Huang[2,3]

[1]Key Laboratory for Biorheological Science and Technology, Ministry of Education, College of Bioengineering, Chongqing University, Chongqing, People's Republic of China; [2]School of Sports and Health Science, Tongren University, Tongren, People's Republic of China; [3]School of Physical Education, Guangxi University of Science and Technology, Guangxi, People's Republic of China

Correspondence: Jun Pan; Xiao Huang, Tel/Fax +86023-65102507, Email panj@cqu.edu.cn; humphrey8531@hotmail.com

Purpose: Photodynamic therapy (PDT) is a non-invasive therapeutic modality that is used for several types of cancer and involves three essential elements (light, photosensitizer (PS), and oxygen). However, clinical PS is limited by the low yield of reactive oxygen species (ROS) and a long retention time. Therefore, developing a low-cost PS that can significantly increase ROS yield in a short time is of utmost importance.

Methods: In this study, brusatol (Bru) was loaded on the surface of ultraviolet A (UVA)-responsive zinc oxide (ZnO)-coated magnetic nanoparticles (Fe_3O_4@ZnO-Bru). The PS was well characterized by transmission electron microscopy (TEM), Fourier Transform infrared spectroscopy (FTIR), a superconducting quantum interference device, and dynamic light scattering (DLS). 3-(4,5-Dimethyl-2-thiazolyl)-2,5-diphenyl-2-*H*-tetrazolium bromide (MTT) and Hoechst staining were used to determine the inhibitory effect of Fe_3O_4@ZnO-Bru on squamous cell carcinoma cells (SCC) with or without UVA radiation. Intracellular ROS levels and expression of the Nrf2 signaling pathway were also determined.

Results: FTIR showed that Bru was successfully loaded on Fe_3O_4@ZnO. Fe_3O_4@ZnO-Bru was superparamagnetic, and the zeta potential was 8.86 ± 0.77 mV. The Bru release behavior was controlled by UVA. Fe_3O_4@ZnO-Bru with UVA irradiation induced an increase of 48% ROS productivity compared to Fe_3O_4@ZnO-Bru without UVA irradiation, resulting in a strong inhibitory effect on SCC. Furthermore, Fe_3O_4@ZnO-Bru nanocomposites (Fe_3O_4@ZnO-Bru NCs) had nearly no toxic effect on healthy cells without UVA radiation. The released Bru could significantly inhibit the Nrf2 signaling pathway to reduce the activity of scavenging excess ROS in SCC.

Conclusion: In this study, Fe_3O_4@ZnO-Bru was successfully synthesized. PDT was combined with photochemotherapy, which exhibited a higher inhibitory effect on SCC. It can be inferred that Fe_3O_4@ZnO-Bru holds great potential for skin SCC therapy.

Keywords: UVA-triggered chemotherapy, photodynamic therapy, reactive oxygen species, magnetic targeting

Introduction

Cutaneous squamous cell carcinoma (SCC), the second most common type of skin cancer, is a metastatic cancer that originates from squamous cells located in the suprabasal epidermis.[1] Although chemotherapy is widely used in the treatment of skin cancer,[2] it often causes a weakened immune system, significant side effects, and low drug efficacy due to the poor targeting ability of chemotherapeutics.[3] Therefore, it is important to improve the targeting ability of chemotherapeutics to improve their treatment effect and reduce side effects.[4] Photodynamic therapy (PDT) as a minimally invasive treatment modality[5] possesses important characteristics including selective localized treatment, target specific selectivity, and fewer side effects.[6] In this study, photosensitizer (PS) was administered and subsequently activated by illumination with exciting light at the target site. The activated PS reacts with available oxygen to form reactive oxygen species (ROS), which induce tumor cell death and vascular shutdown. The therapeutic effect of PDT

Received: 26 April 2022
Accepted: 11 July 2022
Published: 1 August 2022

depends on the generation of a sufficient amount of ROS.[7] In addition, after intravenous injection of PS, patients need to stay in a dark environment until the PS is eliminated from the body because the eyes of patients are sensitive to indoor bright light or sunlight and their skin is readily sunburned, swollen, and blistered when exposed to bright light for a short period of time.[8] Furthermore, damage to healthy tissues as well as cutaneous photosensitivity can occur. Therefore, increasing the amount of ROS as well as the targeting ability of PS are effective means to improve the efficacy of PDT.

Zinc oxide (ZnO) is a common metal oxide that is non-toxic and of low cost.[9] Its cellular toxicity could be activated by UVA irradiation, which enables ZnO to be a potential PS in clinical applications.[10] Indeed, when semplice ZnO nanoparticles were exposed to UVA light, they exhibited some toxicity to several types of cancer cells.[11,12] However, the amount of ROS was erratic, due to the different sizes of ZnO nanoparticles, and did not meet clinical requirements. Fortunately, ZnO nanoparticles not only exhibit ultra-high drug-loading efficiency but also high-performance intracellular delivery of chemotherapeutics.[13] Chemotherapeutics can couple with the photo-toxicity of ZnO to induce cell death. Furthermore, in our previous studies,[14,15] we found that ZnO nanoparticles were UVA-responsive and could transfer from a hydrophobic state to a hydrophilic state to accurately control the release of loaded drugs. In this way, it is easy to realize combined chemo and PDT controlled by UVA radiation. Bru is a quassinoid isolated from the *Brucea javanica* plant and has extensive pharmacological activities, such as anti-inflammatory and antitumor activities.[16] Recently, it was reported that Bru is a potent inhibitor of Nrf2 activation, thereby ultimately leading to tumor growth inhibition and ameliorated chemoresistance.[17] Bru regulated the Nrf2 signaling pathway by reducing the level of Nrf2 factor in cancer cells, and weakened the antioxidant ability of cells, resulting in increasing the accumulation of intracellular ROS.[18] Herein, we intended to employ ZnO-coated iron oxide core-shell nanocomposites (Fe_3O_4@ZnO NCs) to carry Bru as a novel PS. This PS not only owns favorable magnetic targeting property but also intelligently controls the release of Bru under the irradiation of UVA to show a synergistic effect combined with the photo-toxicity of ZnO (Figure 1). We hypothesize that this PS shows synergistic photo-toxicity to improve the therapeutic effect and targeting ability to reduce side effects.

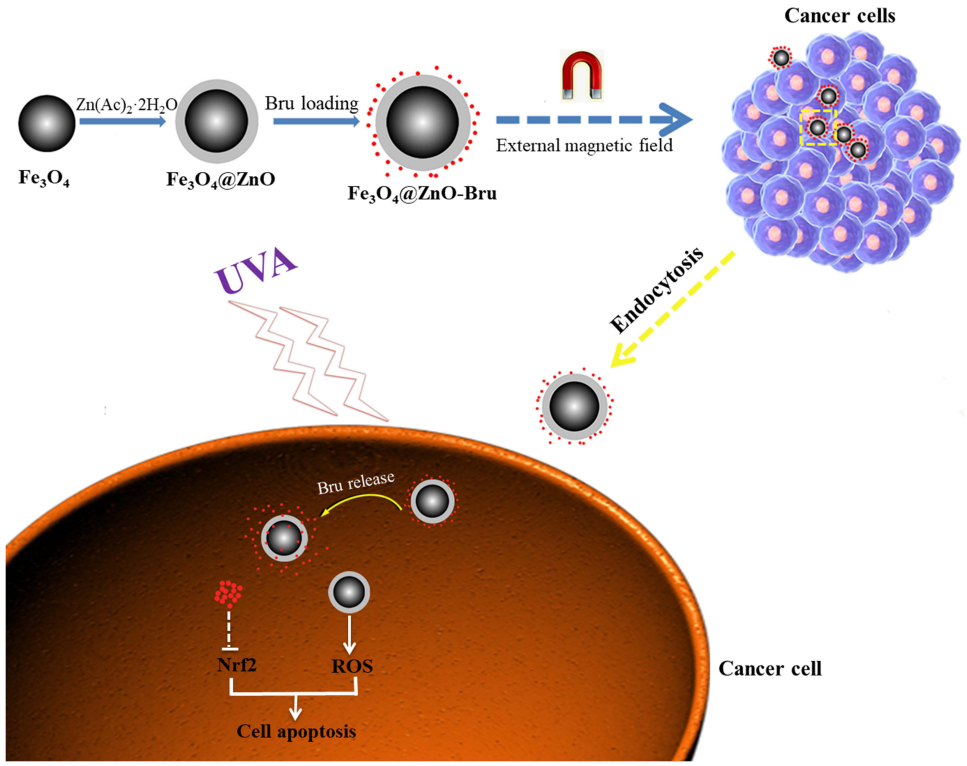

Figure 1 The illustration of the preparation and inhibitory mechanism Fe_3O_4@ZnO-Bru. Such novel PS is easily to realize combined chemo and photodynamic therapy controlled by UVA radiation.

Therefore, in this study, we synthesized and characterized Fe_3O_4@ZnO-Bru and studied their UVA-controlled drug release behavior. The anti-cancer effect and its inhibitory mechanism of Fe_3O_4@ZnO-Bru for combined chemo and PDT were investigated. Moreover, the biocompatibility of Fe_3O_4@ZnO-Bru was evaluated.

Materials and Methods

Materials

$FeCl_3$•$6H_2O$ (AR, Kelong, China), $FeCl_2$•$4H_2O$ (AR, Damao, China), ethanol, and acetone (AR, Chuandong, China), zinc acetate dihydrate ($Zn(Ac)_2$•$2H_2O$)(AR, Gracia, China), phosphate-buffered saline (PBS), penicillin–streptomycin (PS) (Dingguo, China), fetal bovine serum (FBS) (NTC, Logan, USA), trypsin (Hyclone, Logan, USA), RPMI 1640 (Gibco, New York, USA) and 3-(4,5-dimethyl-2-thiazolyl)-2,5-diphenyl-2-*H*-tetrazolium bromide (MTT, Solarbio, Beijing, China) were used as received unless otherwise noted. Hoechst staining kit (C0003) and a reactive oxygen species (ROS) assay kit (S0033) were purchased from Beyotime Biotechnology (Shanghai, China). RIPA lysis buffer, SDS lysis buffer, phenylmethylsulfonyl fluoride, and a BCA protein assay kit (P0010) used for Western blot analysis were purchased from Beyotime Biotechnology (Shanghai, China). Nrf2 (#12121), NQO1 (#3187), HO-1 (#43966), GSTP1 (#3369), and NF-κB (#8242) primary antibodies were obtained from Cell Signaling Technology (USA). GAPDH antibody (BM1623) was purchased from Wuhan Boster Biological Technology (Wuhan, China). Brusatol was purchased from Chengdu Desite Biotechnology (Chengdu, China). For all experiments, ultrapure deionized water (Millipore, Massachusetts, USA) was used. Immortalized human skin keratinocytes (HaCaT cells) and squamous carcinoma cells (SCC) were received as a valuable gift from Prof. Li Zhong, and human umbilical vein endothelial cells (HUVECs) were kindly provided by Prof. Kaiyong Cai in our affiliation. All cell lines were conducted under the approval of the Ethics Committee of Chongqing University.

Optimizing the Adsorption of Brusatol

Fe_3O_4 cores were synthesized by a co-precipitation method. Briefly, under the protection of N_2, $FeCl_3 \cdot 6H_2O$ and $FeCl_2 \cdot 4H_2O$ were reacted in an HCl aqueous solution and then in a NaOH solution to generate Fe_3O_4. Next, $Zn(Ac)_2 \cdot 2H_2O$ was added, and Fe_3O_4@ZnO was obtained by an oil bath at 160 °C for 1.5 h. This method is detailed in our previously published article.[19] Various masses of previously synthesized Fe_3O_4@ZnO NCs (W: W=100:1, 50:1, 10:1, 1:1, 1:10, 1:50, 1:100, Fe_3O_4@ZnO: Bru) fully dispersed in an aqueous solution, then added into the acetone containing a corresponding amount of Bru, respectively. Then, the solution was ultrasonically shocked for 1h. After centrifugation at 30,000 rpm for 10 min, the concentration of Bru in the supernatant was determined by measuring the absorbance at 590 nm using a UV-VIS spectrophotometer. Accordingly, the adsorption rate (AR) and drug loading capacity (DLC) of Bru were calculated referring to the standard curve of Bru in an aqueous solution as follows:

$$\mathrm{AR}(\%) = (Q_t - Q_s)/Q_t \times 100\% \quad (1)$$

$$\mathrm{LC}(\%) = (Q_t - Q_s)/Q_{NCs} \times 100\% \quad (2)$$

Q_t refers to the raw weight of Bru used for adsorption; Q_s refers to the weight of Bru in the supernatant, and Q_{NCs} refers to the raw weight of Fe_3O_4@ZnO used for Bru loading. Experiments were performed in triplicate.

Characterization

The morphology of Fe_3O_4@ZnO NCs and Fe_3O_4@ZnO-Bru NCs was observed by transmission electron microscope (TEM, FEI Tecnai G2 F20, Oregon, USA). Fourier transform infrared spectroscopy (FTIR) spectra of Fe_3O_4@ZnO NCs and Fe_3O_4@ZnO-Bru NCs were determined by a Fourier transform infrared spectrometer (Nicolet iS5, Thermo Fisher, Massachusetts, USA). The magnetization value was determined by a superconducting quantum interference device (MPMS-XL-7, Quantum Design, San Diego, USA). The zeta potential was measured by analyzing 0.1 g of Fe_3O_4 @ZnO/Fe_3O_4@ZnO-Bru NCs in 10 mL of water using the Zetasizer Nano ZS (ZetasizerNano S90, Malvern, UK). All samples were fully dispersed before zeta potential measurement.

UVA-Controlled Bru Release Behavior

Fe_3O_4@ZnO-Bru NCs with an optimal AR were used for a UVA-controlled drug release study. Fe_3O_4@ZnO-Bru NCs were spread evenly on glass slides and were placed in a darkroom equipped with an UVA light therapy system (carnation-58, Lifotronic, 365 nm) at 37 °C. A total of five experimental groups (three samples per group) were prepared. Fe_3O_4@ZnO-Bru NCs were exposed to UVA radiation. At defined time points (1, 2, 4, 6, 8 h), one group of Fe_3O_4@ZnO-Bru NCs was removed and slightly washed with 1 mL of ethanol. The concentration of Bru in ethanol, which was the released Bru from Fe_3O_4@ZnO-Bru NCs, was determined by ultraviolet spectrophotometry and represented the release behavior of Bru. Furthermore, Fe_3O_4@ZnO-Bru NCs without UVA radiation served as a control. Experiments were performed in triplicate.

Cell Culture

HaCaT, HUVEC and SCC cells were cultured in RPMI 1640 medium supplemented with 10% FBS, 100 U/mL of penicillin, and 150 U/mL of streptomycin. Cells were incubated in a humidified cell incubation chamber at 37°C with 5% CO_2. Cells in the exponential growth phase were used for experiments.

Cytotoxicity on Normal Cells

HaCaT and HUVEC cells (3000 per well) were seeded in 96-well plates, grown to 50% confluence, then Fe_3O_4@ZnO-Bru NCs suspension was added at defined concentrations (0.005, 0.01 and 0.05μg/mL). After 2 h, cells were exposed to 100 kJ/m^2 UVA irradiation. A UVA light therapy system (carnation-58, Lifotronic) 365nm (peak) spectrum lamp was used to irradiate the cells following a standard procedure, while non-irradiated cells were used as a background control (control = 0 kJ/m^2). Cells were incubated for another 24 h or 48 h, respectively, then washed with PBS. Subsequently, 90 μL fresh RPMI 1640 medium and 10 μL MTT solution were added to each well followed by incubation at 37°C for 4 h. Next, 110 μL DMSO was added to each well, and the 96-well plate was placed on a shaker at a low speed for 10 min to fully dissolve the crystals. The optical density of the Formazan solution was read on an enzyme-labeled instrument (iMark™ Microplate Reader, Bio-rad680, California, USA) to represent the cellular viability. Untreated cells were used as a positive control to set the cellular viability to 100%. Six parallel samples were prepared for each experiment.

To determine the status of cell survival, a Hoechst staining kit was used. In brief, HaCaT and HUVEC cells were plated in 35-mm cell culture dishes (2×10^4 per dish). After 24 h or 48 h of incubation, the culture solution was discarded, and 1.0 mL of fixation solution (C0003-1, Beyotime, Shanghai, China) was added for 30 min. After removal of the fixative, cells were washed 3 times with PBS on a shaker. HaCaT and HUVEC cells were stained with 0.5 mL Hoechst 33258 dye solution for 20 min, washed three times with PBS solution and observed by inverted fluorescence microscopy (Olympus IX71, Tokyo, Japan).

Inhibitory Effect on Cancer Cells Under UVA Radiation

After overnight incubation of SCC, Fe_3O_4@ZnO-Bru NCs, Bru, and Fe_3O_4@ZnO NCs at defined concentrations (the concentration of Fe_3O_4@ZnO-Bru NCs added was 0.005, 0.01, 0.05μg/mL, Bru and Fe_3O_4@ZnO NCs were added according to the DLC) were added into the culture medium. After 2 h, cells were exposed to 100 kJ/m^2 UVA irradiation (Fe_3O_4@ZnO+UVA). Then, cells were incubated for another 24 h or 48 h, respectively. Cells were washed with PBS; then, 90 μL fresh cell culture medium and 10 μL MTT solution were added to each well, followed by incubation at 37°C for 4 h. DMSO (110 μL) was added to each well, and the 96-well plate was placed on a shaker at a low speed for 10 min to fully dissolve the crystals. The optical density of the Formazan solution was read on an enzyme-labeled instrument (iMark™ Microplate Reader, Bio-Rad Model 680, California, USA) to represent the cellular viability. Untreated cells served as the positive control to set the cellular viability to 100%. Six parallel samples were prepared for each experiment.

To determine the status of cell survival, the Hoechst staining kit was used. After 24 h or 48 h of incubation, the culture solution was discarded, and 1.0 mL of fixation solution was added for 30 min. Then, the fixative was removed, and cells were washed 3 times with PBS on a shaker. SCC cells were stained with 0.5 mL Hoechst 33,258 dye solution for 20 min, washed three times with PBS, and observed by inverted fluorescence microscopy.

Detection of Intracellular Oxygen Radicals

The production of ROS in solution was routinely detected by a ROS assay kit according to the manufacturer's instructions. In brief, SCC cells were seeded in 35-mm cell culture dishes at a density of 1×10^5 cells per dish and incubated at 37°C overnight. Next, Fe_3O_4@ZnO NCs, Bru, and Fe_3O_4@ZnO-Bru NCs were added at different concentrations (see section *Inhibitory effect on cancer cells under UVA radiation*). After 2 h, cells were treated with 100 kJ/m^2 UVA irradiation. After being incubated for another 24 h or 48 h, 10 μM of 2′,7′-dichlorodihydrofluorescein diacetate (DCFH-DA) was added to the cells. After 30 min, cells were washed with PBS and collected. The fluorescence intensities of the cells, which indicated their ROS levels, were recorded by flow cytometry (CytoFLEX, Beckman, Florida, USA) at excitation and emission wavelengths of 488 and 525 nm, respectively. Three parallel samples were prepared for each experiment.

Western Blot Analysis

The treatment method of SCC cells was similar to the method described in section *Inhibitory effect on cancer cells under UVA radiation*. After incubation for 24 h, cells were lysed in RIPA lysis buffer. To determine the various proteins, cell lysates were prepared using extraction with SDS lysis buffer in the presence of 1 mM phenylmethylsulfonyl fluoride (PMSF). The protein concentration was measured by a BCA protein assay kit (P0010, Beyotime, Shanghai, China), and 10 μg protein per lane was separated by SDS-PAGE on an electrophoresis apparatus (PowerPac^{TM} Basic, Bio-rad, California, USA) and transferred to polyvinylidene difluoride membranes. After transfer, membranes were blocked with 5% nonfat milk in Tris-buffered saline tween (TBST, T1086, Solarbio, Beijing, China) for 2 h at room temperature and incubated with respective primary antibodies (Nrf2, HO-1, GSTP1, NQO1, NF-κB, GAPDH) overnight at 4°C. Membranes were washed three times with 1×TBST and incubated with horseradish peroxidase-conjugated secondary antibodies. The electrophoresis instrument was purchased from Bio-rad (PowerPac^{TM} Basic, California, USA). Signals were recorded by ECL reagent (#34095, Thermo Scientific, Massachusetts, USA) and visualized by AZURE Biosystems (c300, California, USA).

Xenograft Assay in Nude Mice

Athymic nude (nu/nu) mice were obtained from the Chongqing Medical University (Chongqing, China). All animal experiments were conducted under the Animal Management Rules of the Ministry of Health of the People's Republic of China (Document No. 55, 2001). In brief, 4-week-old male mice were injected with SCC cells (3×10^6 cells) in the right flank and into the subdermal space. Once tumors reached a mean volume of 30–50 mm^3, mice were randomly allocated into two groups and treated with either PBS (control group) or nanocomposites with UVA (100kJ/m^2) every other day for 16 days.

Statistical Analysis

Statistical analyses were performed using GraphPad Prism 8.0 for Windows (La Jolla, CA, USA). The results are presented as the mean ± SEM. The significance of all experiments was determined by one-way ANOVA plus Bonferroni posttest analysis ($p<0.05$).

Results and Discussion

Preparation and characterization of Fe_3O_4@ZnO-Bru NCs

TEM confirmed the core-shell structure of Fe_3O_4@ZnO NCs, which was analogously square and monodisperse (Figure 2A). After Bru loading, no obvious changes were observed in morphology and size (Figure 2B). The size of the Fe_3O_4@ZnO NCs and Fe_3O_4@ZnO-Bru NCs was in the range of 7–10 nm as determined by electron microscopy. The FTIR results of Fe_3O_4@ZnO NCs and Fe_3O_4@ZnO-Bru NCs are shown in Figure 2C. Compared to the spectrum of Fe_3O_4@ZnO NCs, the adsorption at 1740.30 cm^{-1} and 1682.24 cm^{-1} showed the existence of –COO– and C=O, respectively. Several intense bands are present around 2954.48 cm^{-1}, resulting from the increment of –CH_3. The adsorption at 1295.87 cm^{-1} indicated the existence of –OH. All FTIR results displayed that Bru was successfully loaded on the surface of Fe_3O_4@ZnO NCs. The magnetization curves of Fe_3O_4@ZnO NCs and Fe_3O_4@ZnO-Bru NCs demonstrated that they are superparamagnetic because there was no hysteresis and both their remanence and coercivity were zero (Figure 2D). Despite the saturation of Fe_3O_4@ZnO-Bru NCs decreased to 33.56

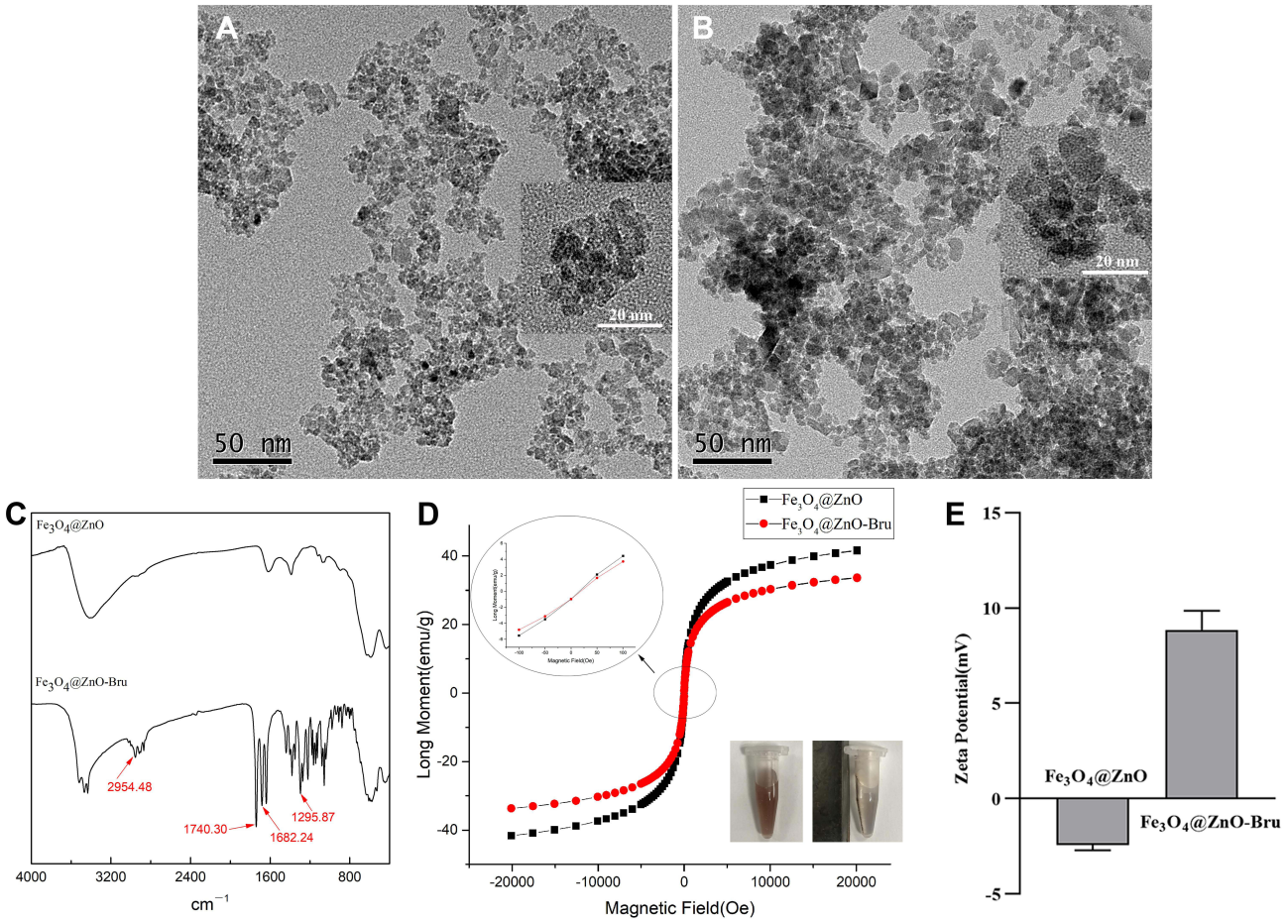

Figure 2 Characterization of Fe_3O_4@ZnO NCs and Fe_3O_4@ZnO-Bru NCs. (**A** and **B**) TEM images of Fe_3O_4@ZnO NCs (**A**) and Fe_3O_4@ZnO-Bru NCs (**B**). Scale bar: 50 nm. Insert: TEM image with a larger magnification, scale bar: 20 nm; (**C**) FTIR of Fe_3O_4@ZnO NCs and Fe_3O_4@ZnO-Bru NCs; (**D**) Magnetic hysteresis loops of Fe_3O_4@ZnO NCs and Fe_3O_4@ZnO-Bru NCs. The saturation of Fe_3O_4@ZnO-Bru slightly decrease compared with Fe_3O_4@ZnO but is still superparamagnetic, indicating that our drug delivery systems have the potential to be directed to a certain area by externally applied magnetism. Insert: The NCs solution was changed from stable to aggregated state under the magnetic field; (**E**) Zeta potential.

emu•g^{-1} due to the loading of Bru in comparison with the 41.50 emu•g^{-1} of Fe_3O_4@ZnO, their magnetic response was not influenced because they were gathered together within 5 min under an external magnetic field (Figure 2D insert), which indicated a great magnetic response ability. In consideration of other nano biomaterials based on Fe_3O_4@ZnO,[20,21] it can be inferred that Fe_3O_4@ZnO-Bru NCs had good magnetic separating and targeting properties. They, therefore, have the potential of magnetic targeting. In addition, the zeta potential changed from −2.43 ± 0.21 mV (Fe_3O_4@ZnO NCs) to 8.86 ± 0.77 mV (Fe_3O_4@ZnO-Bru NCs) (Figure 2E). The drug-loaded nanocomposites were positively charged, and because the outside of the cell membrane also has a positive charge, it is not easily adsorbed by cells, and can only be localized to cancer cells through magnetic targeting.

Taken together, these observations indicated that Fe_3O_4@ZnO-Bru NCs could be localized by an externally applied magnetic field in a desired region, such as the SCC area to realize a targeting function and decrease side effects in healthy tissues.[22]

UVA-Controlled Drug Release

Realizing UVA-controlled drug release is key in designing our Fe_3O_4@ZnO-Bru NCs to realize combined chemotherapy and PDT. Thus, the UVA-controlled Bru release behavior was studied. A UVA light therapy system 365 nm spectrum lamp was used. Under the initial UVA radiation for 1 h, 82.96±1.82% of Bru was released from Fe_3O_4@ZnO-Bru NCs, while nearly no Bru was released without UVA irradiation (Figure 3).

In our previous studies, we found that the surface of ZnO could release the adsorbed drug in a controlled manner via UVA irradiation: Fe_3O_4@ZnO NCs could intelligently control and release the loaded drug depending on the conversion

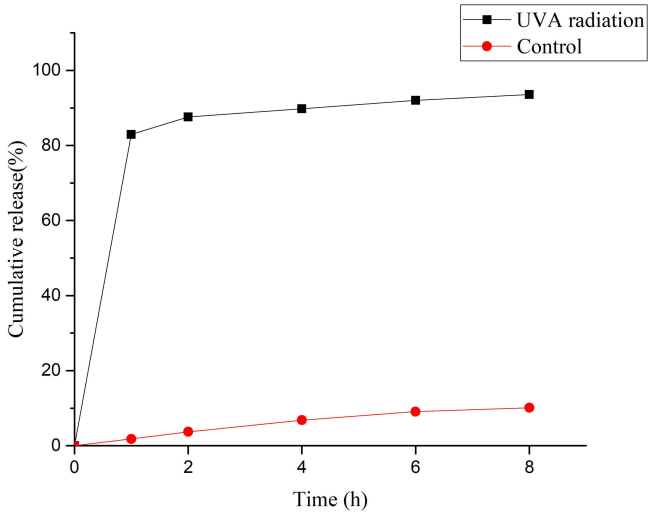

Figure 3 The UVA-controlled release behavior of Fe_3O_4@ZnO-Bru NCs.

of hydrophilic/hydrophobic of ZnO shell under UVA irradiation.[15,23] In the absence of UVA irradiation, the drug was still adsorbed on ZnO shell and not released from the carrier. In recent years, ZnO nanoparticles have been preferable drug delivery carriers.[24,25] Light-responsive drug delivery systems have attracted more interest due to the controllable stimuli. The trigger is easily steerable in emitted energy and range of exposure. Based on this, ZnO was chosen as the appropriate carrier to prepare UVA-responsive drug delivery systems. In this study, Fe_3O_4@ZnO NCs were used for Bru loading and UVA-controlled release. Moreover, it is very possible to realize combined chemotherapy and PDT for enhanced treatment of SCC using Fe_3O_4@ZnO-Bru NCs.

Cytotoxicity of Fe_3O_4@ZnO-Bru on HaCaT Cells and HUVEC

To evaluate the biocompatibility of Fe_3O_4@ZnO-Bru NCs, their cytotoxicity on HaCaT cells and HUVEC was determined. The relative viability of HaCaT and HUVEC cells was measured by conducting MTT assays in the presence of Fe_3O_4@ZnO-Bru NCs at concentrations of 0.005, 0.01, and 0.05 mg/mL. When the cells were co-cultured with Fe_3O_4@ZnO-Bru NCs after 24 h or 48 h, Fe_3O_4@ZnO and Fe_3O_4@ZnO-Bru NCs did not display obvious toxicity on HaCaT cells and HUVEC (Figure 4). The cellular viability was above 80% in all the experimental groups, which was deemed to

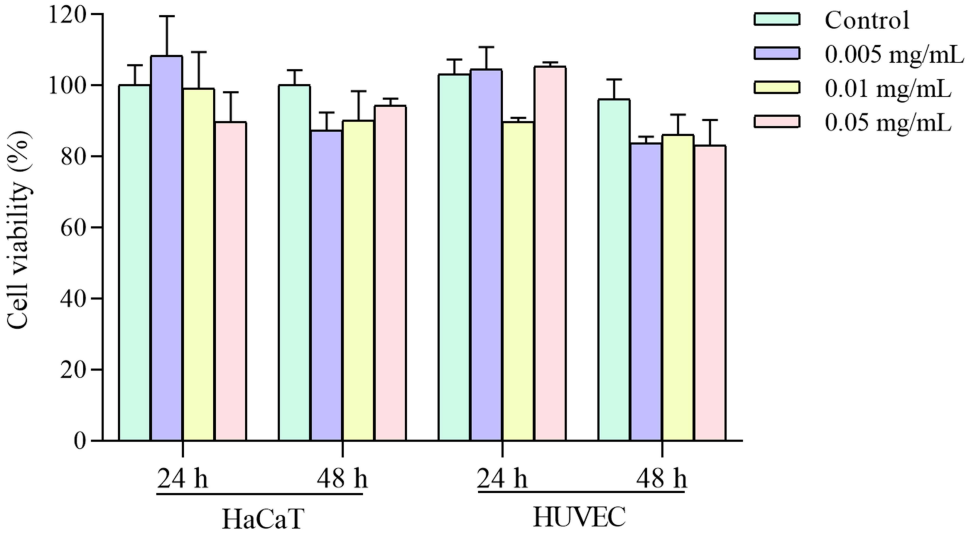

Figure 4 The cytotoxicity of Fe_3O_4@ZnO-Bru NCs on HaCaT and HUVEC cells with different concentrations.

have nearly no toxicity to HaCaT cells and HUVEC. Accordingly, we believe our Fe_3O_4@ZnO-Bru NCs would be safe drug delivery systems for cancer treatment with few side effects.

Figure 5 shows the morphology of HaCaT cells (Figure 5A) and HUVEC (Figure 5B) cells treated with Fe_3O_4@ZnO-Bru NCs at a concentration of 0, 0.005, 0.01 and 0.05 mg/mL. When Fe_3O_4@ZnO-Bru NCs were cultured with HaCaT cells and HUVEC after 24 or 48 h, the morphology of the cells was not affected compared to untreated cells, thereby indicating that HaCaT cells and HUVEC grew exuberantly with Fe_3O_4@ZnO-Bru NCs.

Furthermore, Hoechst staining was used to determine the status of cell survival. The results of the ratio of viable cells are shown in Figure 6. The ratio of all groups was approximately 85%, which was consistent with the cytotoxicity results. Figure S1 shows the fluorescence images of HaCaT cells (Figure S1A) and HUVEC (Figure S1B) treated with Fe_3O_4@ZnO-Bru NCs after Hoechst 33,342 staining. After being co-cultured with Fe_3O_4@ZnO-Bru NCs for 24 or 48 h, HaCaT cells and HUVEC emitted bright blue fluorescence, indicating that HaCaT cells and HUVEC grew exuberantly under these conditions. These results are in accordance with the cell morphology results. Thus, the results demonstrated good biocompatibility of Fe_3O_4@ZnO-Bru NCs.

Biocompatibility is a key concern of biomaterials for their applications in the clinic. In this study, the cytotoxicity assay was used to evaluate the potential application of Fe_3O_4@ZnO-Bru NCs on the skin. In this study, the MTT assay, cell morphology, and Hoechst staining were carried out for cytotoxicity evaluation. The results showed that Fe_3O_4@ZnO-Bru NCs had little cytotoxicity. After 48 h of co-incubation with Fe_3O_4@ZnO-Bru NCs, the cell viability was still above 82%. Fe_3O_4@ZnO-Bru NCs exhibit better performance in the cell survival rate compared with other nanoparticles, such as TiO_2 NPs, incubation with HaCaT cells for 24 h with the concentration of 0.005 mg/mL, cellular viability was less than 75%.[26] In addition, incubation of 0.01 mg/mL SiO_2 nanoparticles with HaCaT cells for 24 h resulted in

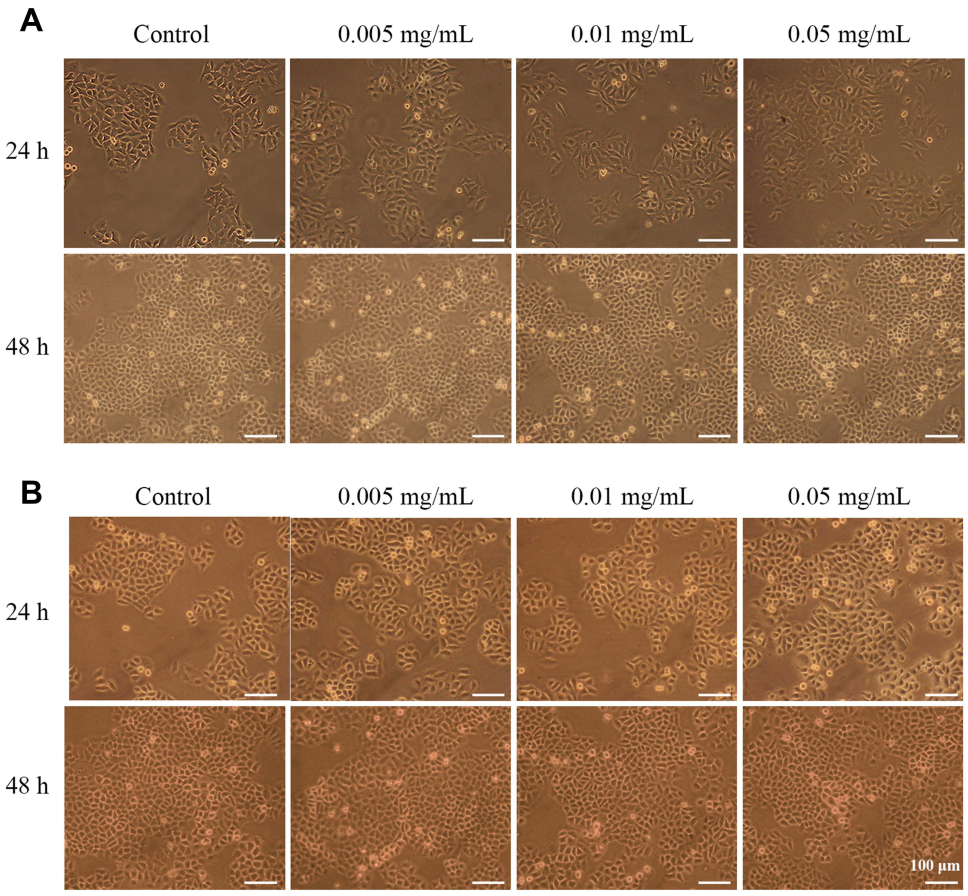

Figure 5 Cellular morphology images. HaCaT cells (**A**) and HUVEC cells (**B**) were treated with Fe_3O_4@ZnO-Bru NCs for 24 or 48 h with the concentration of 0 mg/mL, 0.005 mg/mL, 0.01 mg/mL and 0.05 mg/mL.

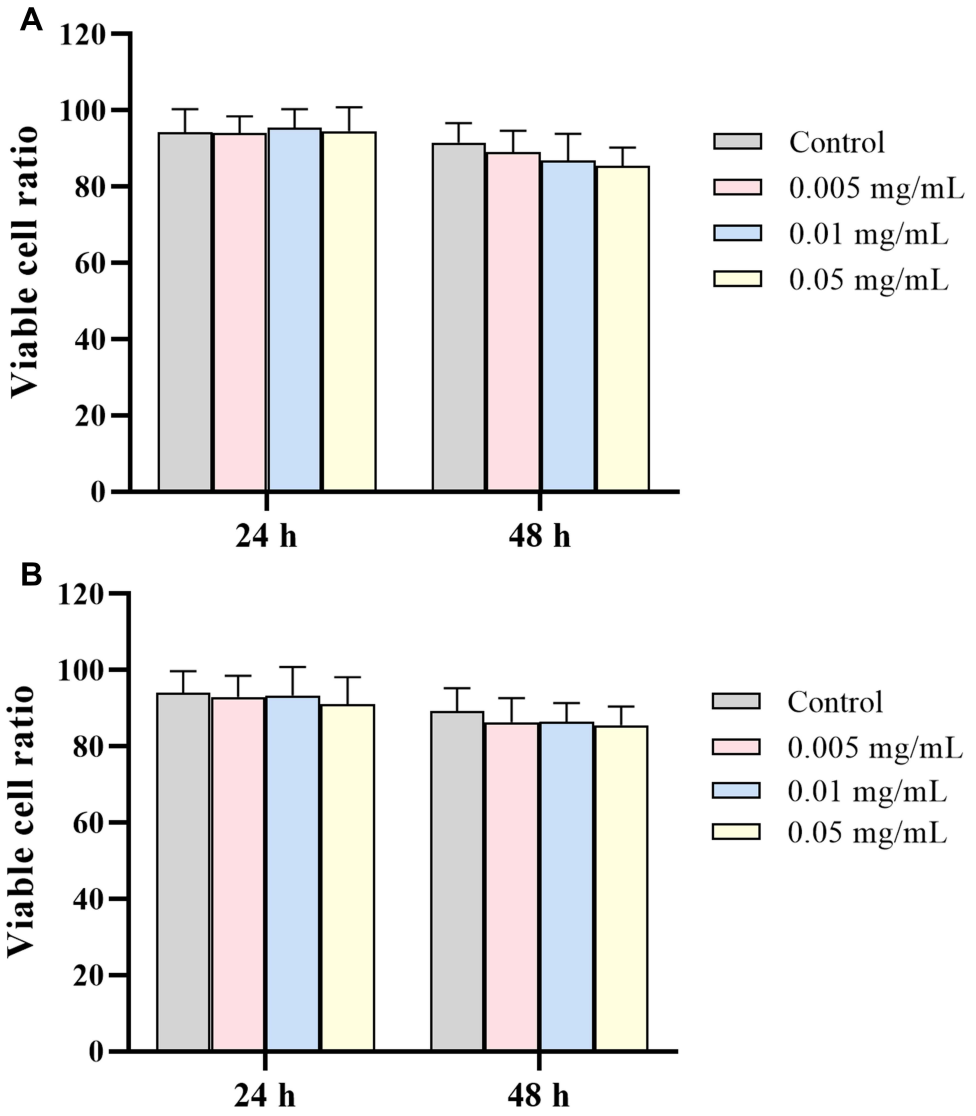

Figure 6 The ratio of viable cells. HaCaT cells (**A**) and HUVEC cells (**B**) were treated with Fe_3O_4@ZnO-Bru NCs for 24 or 48 hours with the concentrations of 0 mg/mL, 0.005 mg/mL, 0.01 mg/mL and 0.05 mg/mL.

a cellular viability of about 80%, which was similar to the cell viability of our 0.01 mg/mL nanocomposites when incubated for 48 h.[27] Overnight (24 h) viability decreased less than 50% at an iron concentration of 1 nM for both citrate-IONP (citrate-Iron oxide nanoparticles) and dextran-IONP (dextran-Iron oxide nanoparticles).[28] Thus, our Fe_3O_4@ZnO-Bru NCs have a toxicity that is similar to that of low-toxic superparamagnetic iron oxide nanoparticles (SPIONs), which, when incubated with HUVEC cells for 24 h at a concentration of 37.5 μg/mL and 75 μg/mL, resulted in a cell viability of 80%.[29] These findings show that our nanocomposites have good biocompatibility.

Inhibition of Fe_3O_4@ZnO-Bru to SCC Cells in vitro

To evaluate the effectiveness of chemotherapy combined with PDT of Fe_3O_4@ZnO-Bru NCs, the influence of Fe_3O_4@ZnO-Bru NCs on the growth of SCC cells was investigated after UVA radiation. The inhibition rate of the 0.05 mg/mL Fe_3O_4@ZnO-Bru+UVA group was 60% at 48 h, while that of the 0.05 mg/mL Fe_3O_4@ZnO-Bru group was 14% (Figure 7). It was found that the inhibition rate of the Fe_3O_4@ZnO-Bru+UVA group was up to 4.2-fold greater compared to that of the Fe_3O_4@ZnO-Bru group. The same dose of Fe_3O_4@ZnO had no obvious toxicity to SCC cells after UVA light irradiation, and the cell viability was higher than 75% (Figure S2). Except for the minor effects of UVA radiation on

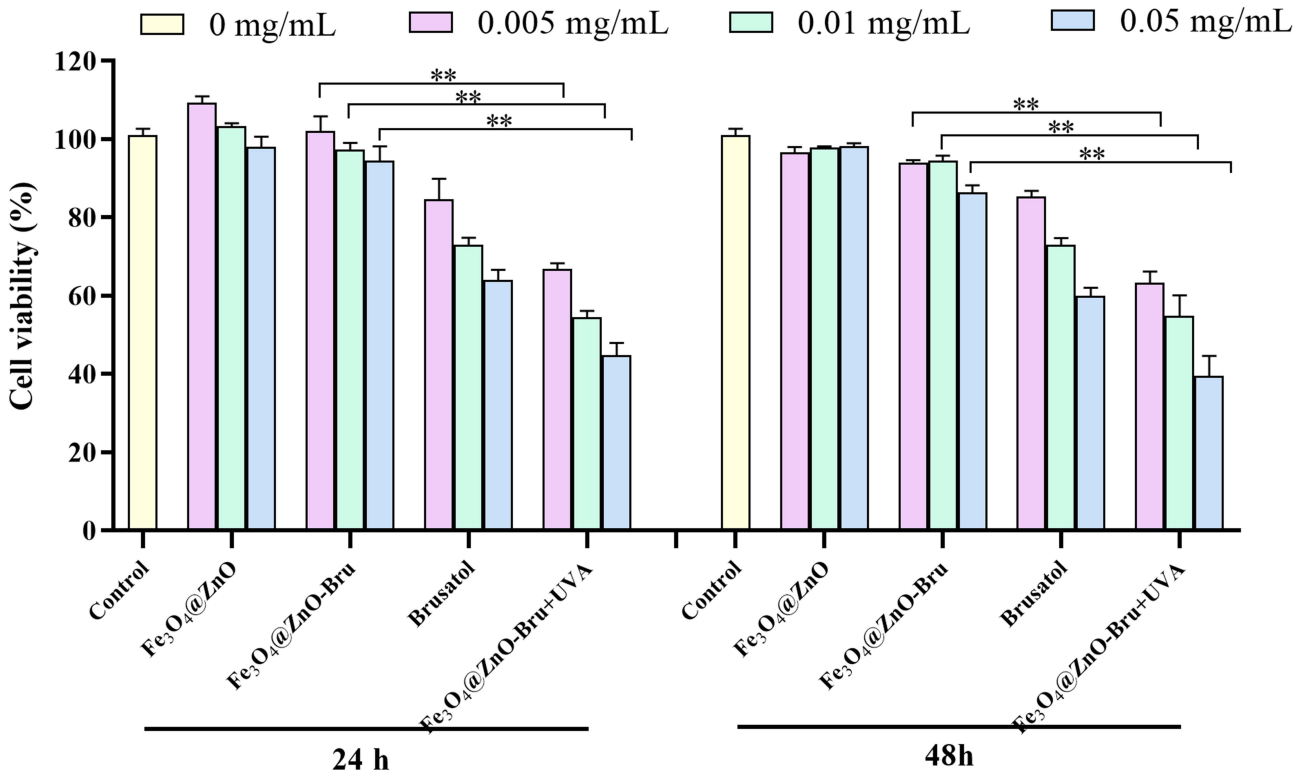

Figure 7 The treatment of Fe_3O_4@ZnO, Fe_3O_4@ZnO-Bru, Bru and Fe_3O_4@ZnO-Bru+UVA to SCC cells. Data are presented as mean ± SD. $^{**}p<0.01$.

the cellular viability (inhibition rate <2.3%[30]), the results confirm the excellent combined therapeutic effect of Fe_3O_4@ZnO-Bru NCs.

Figure 8 shows the morphology images of SCC cells with different treatments after incubation for 24 h (Figure 8A) or 48 h (Figure 8B). Many SCC cells did not adhere to the plate and other cells gathered into masses in Fe_3O_4@ZnO-Bru +UVA group. This phenomenon was much more obvious in Fe_3O_4@ZnO-Bru+UVA group treated with 0.05 mg/mL concentration.

The viable cell ratio of SCC cells is shown in Figure 9. The ratio of live cells in the Fe_3O_4@ZnO and Fe_3O_4@ZnO-Bru groups were both above 90%, and the proportion of live cells in the Bru and Fe_3O_4@ZnO-Bru+UVA groups was decreased. In the Fe_3O_4@ZnO-Bru+UVA group, live cells accounted for about 50% ($p < 0.01$ vs Fe_3O_4@ZnO groups). Figure S3 shows the Hoechst stained images of SCC cells after different treatments and incubation for 24 h (Figure S3A) or 48 h (Figure S3B). The data revealed that more cell death was induced when SCC cells were treated with Bru and Fe_3O_4@ZnO-Bru+UVA. In fact, some dead cells were washed away during Hoechst staining. Thus, the ratio of live cells in the Bru and Fe_3O_4@ZnO-Bru+UVA groups should be lower. These results proved that the combination of chemotherapy and PDT has an additive inhibitory action on SCC cells.

Accumulation of Intracellular ROS Induced by Combination Therapy

Suppression of the Nrf2 signaling pathway causes an increase in ROS and subsequently results in cell death.[31] Therefore, we determined the level of ROS accumulation by SCC cells exposed to Fe_3O_4@ZnO-Bru+UVA. The data showed that Bru and Fe_3O_4@ZnO-Bru+UVA treatment led to a significant increase in ROS in SCC cells (Figure 10A and B). UVA irradiation causes the photosensitizer ZnO to induce cells to produce ROS, and Bru, which has released Fe_3O_4@ZnO-Bru NCs, causes cells to produce ROS. As a result, the Fe_3O_4@ZnO-Bru+UVA group has the highest ROS level.

ROS are closely related to the growth and death of cancer cells.[32,33] ROS can induce DNA mutations and genomic instability, and accelerate the proliferation, immune tolerance as well as metastasis of cancer cells.[34,35] In addition, high ROS levels enhance cellular oxidative stress, which is detrimental to DNA, proteins, and lipids and thereby causes cell

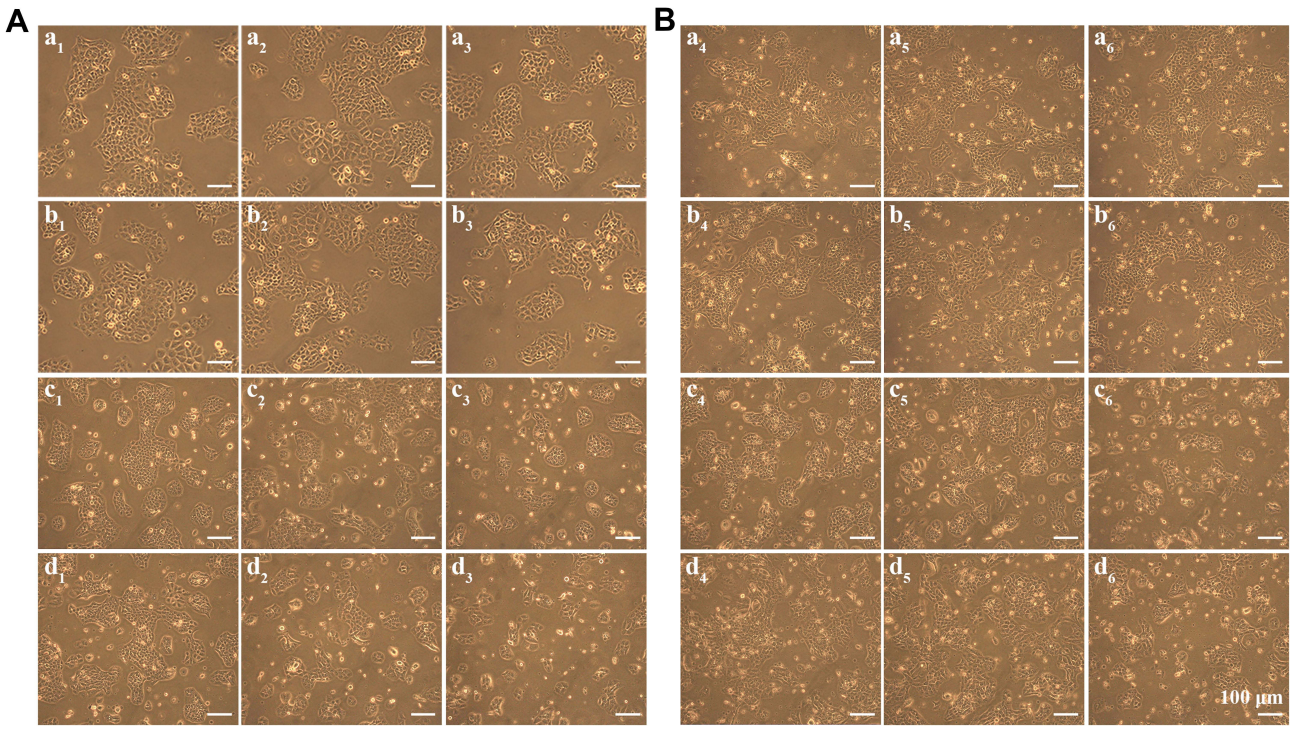

Figure 8 The morphology images of a Fe_3O_4@ZnO, b Fe_3O_4@ZnO-Bru, c Bru, and d Fe_3O_4@ZnO-Bru+UVA treated SCC cells, with the concentrations of 0.005 mg/mL (a_1, b_1, c_1, d_1, a_4, b_4, c_4 and d_4), 0.01 mg/mL (a_2, b_2, c_2, d_2, a_5, b_5, c_5 and d_5) and 0.05 mg/mL (a_3, b_3, c_3, d_3, a_6, b_6, c_6 and d_6) after incubation for 24 h (**A**) or 48 h (**B**).

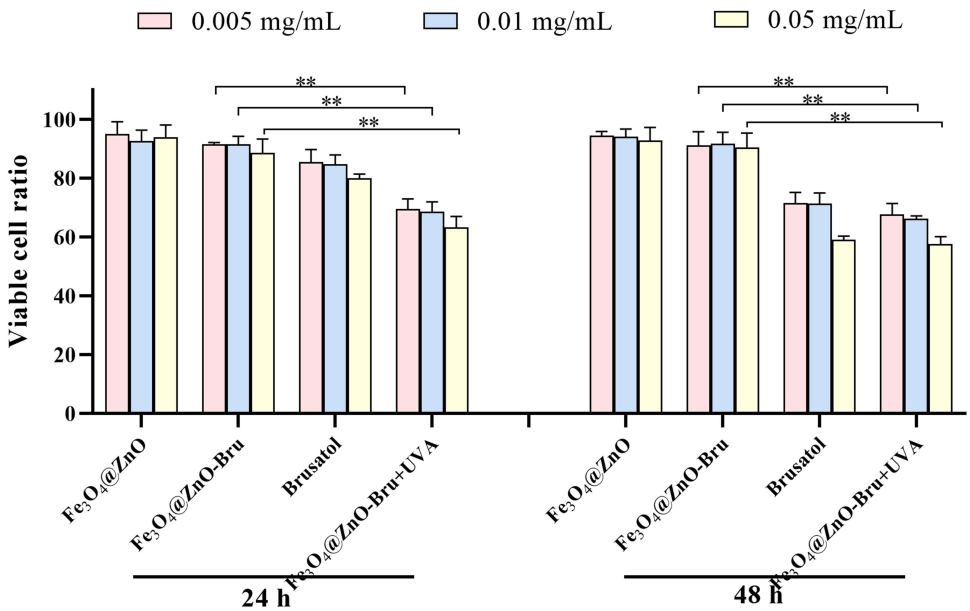

Figure 9 The ratio of viable cells to the total number of cells in the Hoechst image. SCC cells were treated with Fe_3O_4@ZnO, Fe_3O_4@ZnO-Bru, Bru and Fe_3O_4@ZnO-Bru NCs for 24 and 48 hours with the concentration of 0.005 mg/mL, 0.01 mg/mL and 0.05 mg/mL. Data are presented as mean ± SD. $^{**}p<0.01$.

death.[36,37] Ample studies have shown that inducing cells to produce high concentrations of ROS is a treatment strategy for PDT.[38,39] The Fe_3O_4@ZnO-Bru+UVA prepared in this study not only uses ZnO to produce ROS, but also allows Bru to help reduce the ability of cells to remove ROS, which leads to producing more ROS. Therefore, the reason why many cells in this study, is by significantly increasing the level of ROS. Thus, photochemotherapy plus PDT is more conducive to the treatment of skin SCC.

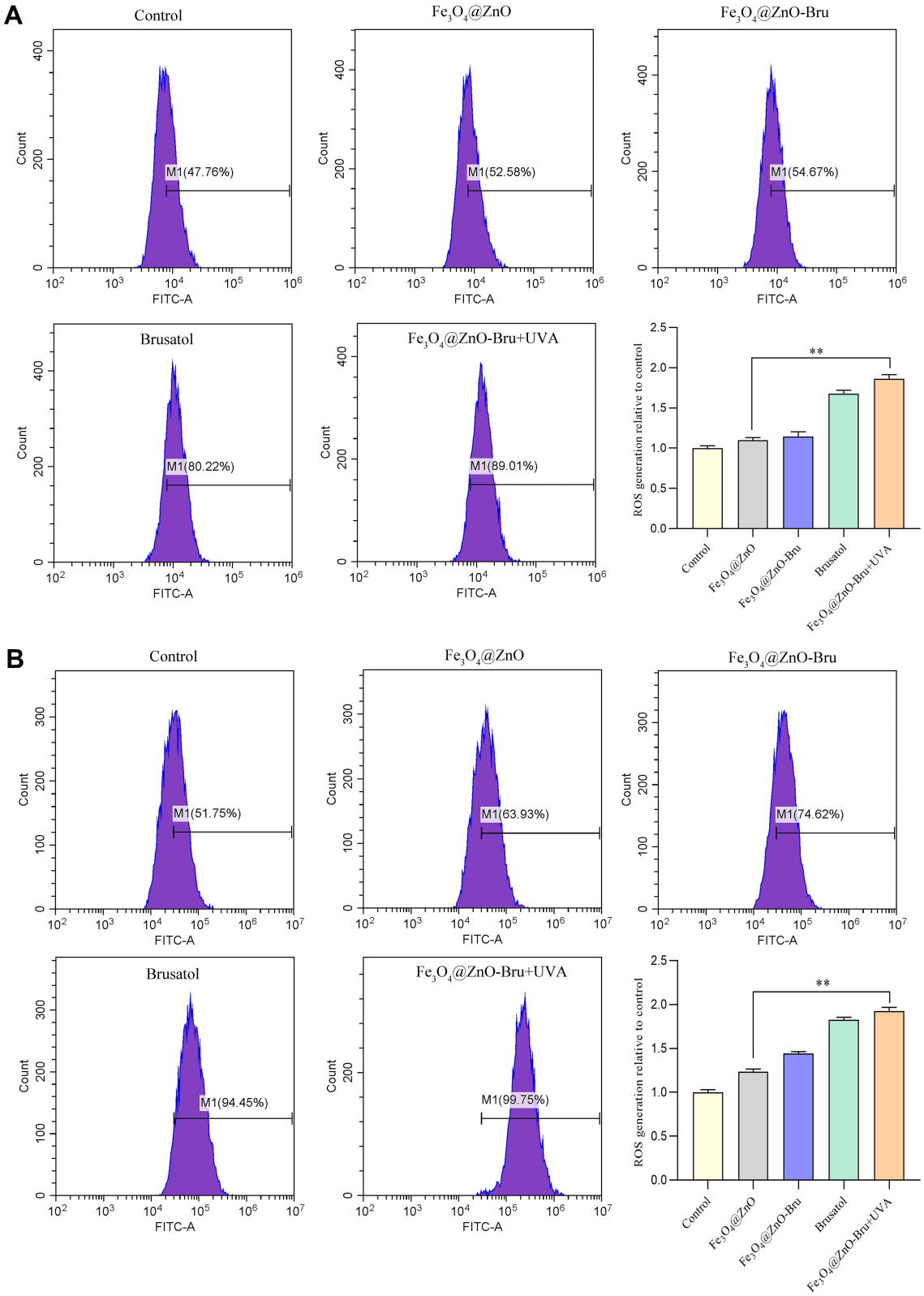

Figure 10 Fe_3O_4@ZnO-Bru NCs responsed to UVA irradiation and increases intracellular ROS level in SCC. SCC cells were treated with Fe_3O_4@ZnO, Fe_3O_4@ZnO-Bru, Bru, or Fe_3O_4@ZnO-Bru+UVA for 24 h (**A**) or 48 h (**B**), and flow cytometry was used to analyze the level of ROS in cells. Bar graphic representation of the fluorescence intensity upon different treatments relative to control were shown. Data are presented as mean ± SD. $^{**}p<0.01$.

Fe_3O_4@ZnO-Bru NCs Inhibit the Nrf2 Signaling Pathway in SCCs

To confirm whether Fe_3O_4@ZnO-Bru inhibit the Nrf2 pathway in SCC cells, whole cell lysates were prepared and protein expression levels were determined by Western blot analysis after cells were treated with Fe_3O_4@ZnO-Bru, Bru, or Fe_3O_4@ZnO-Bru+UVA. After incubation for 24 h, the Fe_3O_4@ZnO-Bru+UVA group showed a reduction in protein levels of Nrf2, HO-1, GSTP1, NQO1 and NF-κB compared to the Fe_3O_4@ZnO-Bru group in SCC cells (Figure 11A and B). Thus, these results suggested that Bru enhanced the antitumor effect of PDT through inhibiting the Nrf2/HO-1 signaling pathway in SCC cells.

In recent years, Nrf2 has been deemed an important and promising target in cancer therapy and many efforts have been made to seek therapeutic strategies directed to block the Nrf2 antioxidant pathway.[40] Bru, as a unique Nrf2 inhibitor, has been shown to regress tumor burden through inhibiting the Nrf2 signaling in several tumor models.[41,42] More importantly, Bru exhibits the potential as an adjuvant drug to enhance the efficacy of chemotherapeutics, such as gemcitabine or cisplatin in pancreatic cancer or lung cancer.[31] In this study, we found that Bru was a potent antitumor compound against SCC cancer cells assisting with PDT. Bru inhibited the Nrf2 pathway, resulting in the inability to clear ROS in time. It caused the therapeutic effect to be enhanced. Notably, the inhibitory effect of Bru combined with PDT on the Nrf2/HO-1 signaling pathway in SCC was identified as a novel mechanism, suggesting a therapeutic advantage for the use of Bru in cancer therapy. Furthermore, the anticancer drug Bru can reduce the level of Nrf2 in SCC cells to negatively regulate the Nrf2 signaling pathway and weaken the antioxidant function of the cells. Therefore, the intracellular ROS level has been accumulated, which may cause greater damage to cancer cells. Thus, using Fe_3O_4@ZnO-Bru NCs to combine chemotherapy with PDT controlled by UVA radiation shows a better therapeutic effect compared with chemotherapy or PDT therapy alone.

Combination Treatment Inhibited Tumor Growth in Nude

To explore the effect of combined chemo and photodynamic cotreatment on tumor growth in vivo, SCC xenografts were grown in Balb/c nude as a heterotopic tumor model. To form a tumor, Balb/c nude were injected with SCC cells (3×10^6 per injection site). After 10 days, the tumor volumes reached of 30–50 mm^3 and nanocomposites with UVA (100 kJ/m^2) were administered to the tumor site every other day for 16 days. Mice were covered with silver paper, and the tumors were irradiated using a UVA lamp. A significant inhibition of tumor growth in vivo was observed after combination treatment (Figure 12) compared with the control group.

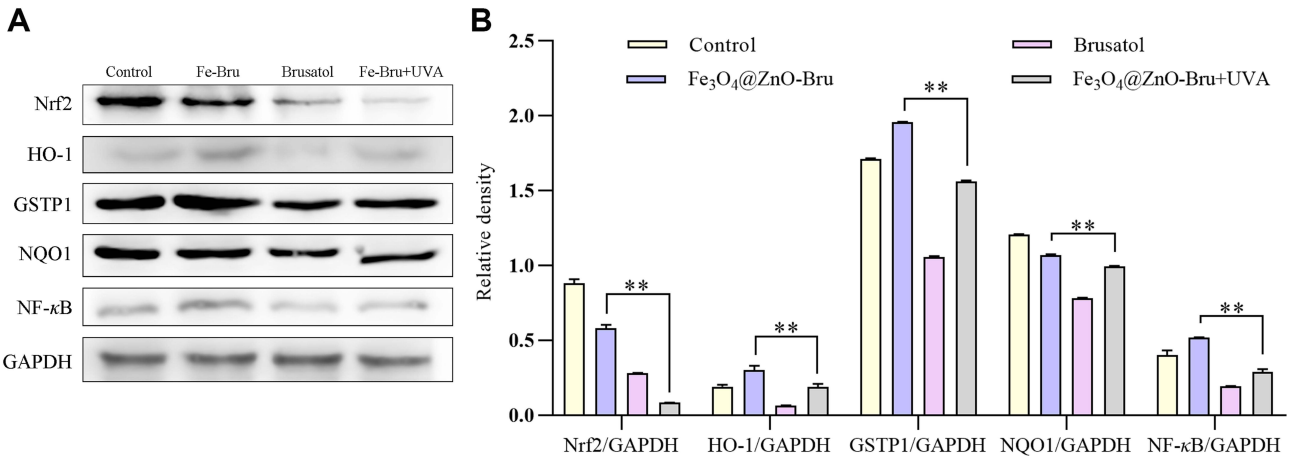

Figure 11 The Fe_3O_4@ZnO-Bru+UVA potently inhibited the activation of Nrf2/HO-1 pathways. (**A**) SCC cells were treated with Fe_3O_4@ZnO-Bru, Bru or Fe_3O_4@ZnO-Bru+UVA for 24 h. The changes in Nrf2/HO-1 signaling pathways were monitored by Western blotting. (**B**) Densitometric analysis was performed on the Western blotting. The levels of Nrf2, HO-1, GSTP1, NQO1 and NF-κB were quantified by using the software Image J. Data are expressed as the mean ± SD of three independent experiments. $^{**}p<0.01$.

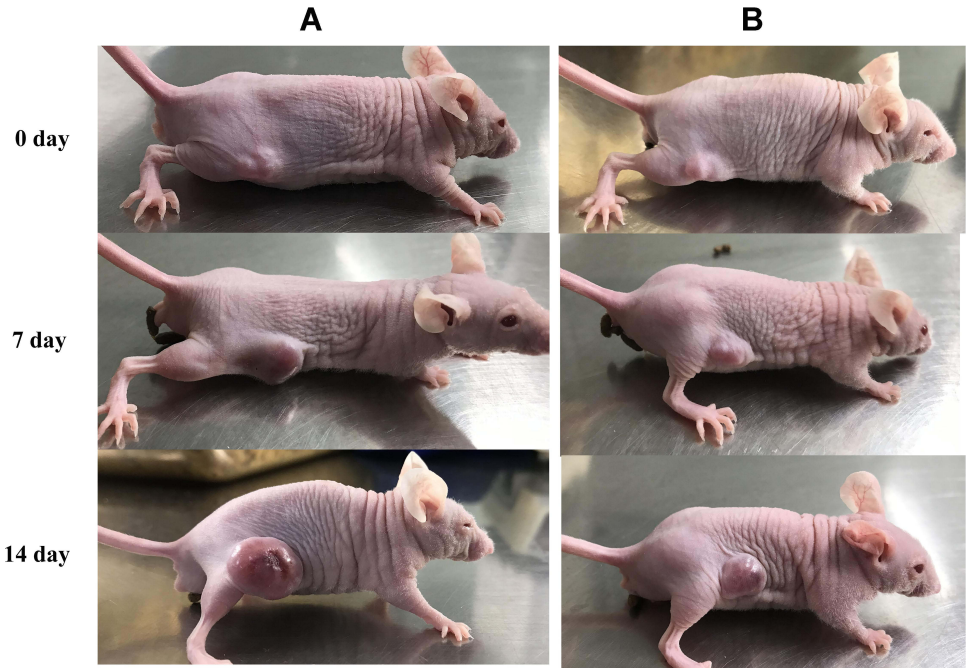

Figure 12 Antitumor efficiency in vivo. Images of SCC tumor-bearing Balb/c nude. (**A**) PBS, (**B**) Fe_3O_4@ZnO-Bru with UVA irradiation.

Conclusion

In this study, Fe_3O_4@ZnO-Bru NPs were successfully synthesized. They show good magnetic targeting performance and biocompatibility. Moreover, their drug release behavior is UVA-responsive, which is easy to realize with combined chemo and dynamic therapy. The combined therapeutic effect for skin cancer treatment is much more efficient compared to chemotherapy or PDT. In addition, it was found that Fe_3O_4@ZnO-Bru could suppress activation of the Nrf2-mediated signaling pathway to decrease the ROS scavenging ability of SCC cells. Therefore, the photo-toxicity of Fe_3O_4@ZnO-Bru increased to perform a more satisfying therapeutic efficacy. Overall, Fe_3O_4@ZnO-Bru have great potential in clinical use for the treatment of cutaneous SCC.

Acknowledgments

This study was supported by the National Natural Science Foundation of China (81860324, 31470902), High-level Innovative Talents in Guizhou Province (2018-2016-023), Fundamental Research Funds for the Central Universities of China (2020CDCGSW051, 2018CDPTCG0001/46).

Disclosure

The authors report no conflicts of interest in this work.

References

1. Kanzaki A, Kudo M, Ansai SI, et al. Insulin-like growth factor 2 mRNA-binding protein-3 as a marker for distinguishing between cutaneous squamous cell carcinoma and keratoacanthoma. *Int J Oncol*. 2016;48(3):1007–1015. doi:10.3892/ijo.2016.3323
2. Li Z, Wang N, Huang C, et al. Downregulation of caveolin-1 increases the sensitivity of drug-resistant colorectal cancer HCT116 cells to 5-fluorouracil. *Oncol Lett*. 2017;13(1):483–487. doi:10.3892/ol.2016.5390
3. Ma Z, Fan Y, Wu Y, et al. Traditional Chinese medicine-combination therapies utilizing nanotechnology-based targeted delivery systems: a new strategy for antitumor treatment. *Int J Nanomed*. 2019;14:2029–2053. doi:10.2147/IJN.S197889
4. Oun R, Moussa YE, Wheate NJ. The side effects of platinum-based chemotherapy drugs: a review for chemists. *Dalton T*. 2018;47:6645–6653. doi:10.1039/C8DT00838H
5. Mascaraque M, Delgado-Wicke P, Damian A, et al. Mitotic catastrophe induced in hela tumor cells by photodynamic therapy with methyl-aminolevulinate. *Int J Mol Sci*. 2019;20(5):1229. doi:10.3390/ijms20051229
6. Yue J, Liang L, Shen Y, et al. Investigating dynamic molecular events in melanoma cell nucleus during photodynamic therapy by SERS. *Front Chem*. 2019;6:665. doi:10.3389/fchem.2018.00665

7. Gu X, Shen C, Li H, et al. X-ray induced photodynamic therapy (PDT) with a mitochondria-targeted liposome delivery system. *J Nanobiotechnol*. 2020;18(1):1–13. doi:10.1186/s12951-020-00644-z
8. Li X, Zheng BY, Ke MR, et al. A Tumor-pH-responsive supramolecular photosensitizer for activatable photodynamic therapy with minimal in vivo skin phototoxicity. *Theranostics*. 2017;7(10):2746–2756. doi:10.7150/thno.18861
9. Chen DW, Lee KY, Tsai MH, et al. Antibacterial application on staphylococcus aureus using antibiotic agent/zinc oxide nanorod arrays/polyethylethylketone composite samples. *Nanomaterials-Basel*. 2019;9(5):713. doi:10.3390/nano9050713
10. Huang X, Du L, Zheng X, et al. Smart Eryc@mZnO nanoparticles with enhanced antibacterial activity under ultraviolet and prolonged antibacterial activity without ultraviolet. *Nanosci Nanotech Let*. 2018;10:1572–1577. doi:10.1166/nnl.2018.2821
11. Luengas S, Marin GH, Aviles K, et al. Enhanced singlet oxygen production by photodynamic therapy and a novel method for its intracellular measurement. *Cancer Biother Radio*. 2014;29(10):435–443.
12. Wahab R, Dwivedi S, Umar A, et al. ZnO nanoparticles induce oxidative stress in Cloudman S91 melanoma cancer cells. *J Biomed Nanotechnol*. 2013;9(3):441–449. doi:10.1166/jbn.2013.1593
13. Wang C, Wen H, Guo H, et al. A novel high doxorubicin-loaded Fe_3O_4@void@ZnO nanocomposite: pH-controlled drug release and targeted antitumor activity. *J Mater Sci*. 2020;55(35):1–12. doi:10.1007/s10853-020-05184-3
14. Huang X, Wang X, Wang S, et al. UV and dark-triggered repetitive release and encapsulation of benzophenone-3 from biocompatible ZnO nanoparticles potential for skin protection. *Nanoscale*. 2013;5(12):5596–5601. doi:10.1039/c3nr00090g
15. Huang X, Nisar MF, Wang M, et al. UV-responsive AKBA@ZnO nanoparticles potential for polymorphous light eruption protection and therapy. *Mat Sci Eng C-Mater*. 2020;107:110254. doi:10.1016/j.msec.2019.110254
16. Yu X, Shang X, Huang X, et al. Brusatol: a potential anti-tumor quassinoid from Brucea javanica. *Chin Herb Med*. 2020;12(4):359–366. doi:10.1016/j.chmed.2020.05.007
17. Ren D, Villeneuve NF, Jiang T, et al. Brusatol enhances the efficacy of chemotherapy by inhibiting the Nrf2-mediated defense mechanism. *P Natla Sci India B*. 2011;108(4):1433–1438. doi:10.1073/pnas.1014275108
18. Wang M, Shi G, Bian C, et al. UVA irradiation enhances brusatol-mediated inhibition of melanoma growth by downregulation of the Nrf2-mediated antioxidant response. *Oxid Med Cell Longev*. 2018;2:1–15.
19. Huang X, Lu J, Yue D, et al. Fe_3O_4@ZnO core-shell nanocomposites for efficient and repetitive removal of low density lipoprotein in plasma and on blood vessel. *Nanotechnology*. 2015;26(12):125101. doi:10.1088/0957-4484/26/12/125101
20. Taufiq A, Ulya HN, Yogihati CI, et al. Effects of ZnO nanoparticles on the antifungal performance of Fe_3O_4/ZnO nanocomposites prepared from natural sand. *Adv Nat Sci-Nanosci*. 2020;11(4):045004.
21. Ammar SH, Abdulnabi WA, Kader H. Synthesis, characterization and environmental remediation applications of polyoxometalates-based magnetic zinc oxide nanocomposites (Fe_3O_4@ZnO/PMOs). *Environ Nano Monit Manage*. 2020;13:100289.
22. Huang X, Yi C, Fan Y, et al. Magnetic Fe_3O_4 nanoparticles grafted with single-chain antibody (scFv) and docetaxel loaded β-cyclodextrin potential for ovarian cancer dual-targeting therapy. *Mat Sci Eng C-Mater*. 2014;42:325–332. doi:10.1016/j.msec.2014.05.041
23. Kong F, Huang X, Yue D, et al. A biocompatible and magnetic nanocarrier with a safe UV-initiated docetaxel release and cancer secretion removal properties increases therapeutic potential for skin cancer. *Mat Sci Eng C-Mater*. 2017;76:579–585. doi:10.1016/j.msec.2017.03.078
24. Zhao Q, Wang J, Zhang Y, et al. A ZnO-gated porphyrinic metal–organic framework-based drug delivery system for targeted bimodal cancer therapy. *J Mater Chem B*. 2018;6(47):7898–7907. doi:10.1039/C8TB02663G
25. Akbarian M, Mahjoub S, Elahi SM, et al. Green synthesis, formulation and biological evaluation of a novel ZnO nanocarrier loaded with paclitaxel as drug delivery system on MCF-7 cell line. *Colloid Surface B*. 2020;186:110686. doi:10.1016/j.colsurfb.2019.110686
26. Lopes VR, Loitto V, Audinot JN, et al. Dose-dependent autophagic effect of titanium dioxide nanoparticles in human HaCaT cells at non-cytotoxic levels. *J NANOBIOTECHNOL*. 2016;14(1):1–13. doi:10.1186/s12951-016-0174-0
27. Yang X, Liu J, He H, et al. SiO_2 nanoparticles induce cytotoxicity and protein expression alteration in HaCaT cells. *Toxicol Lett*. 2010;196(1):S273. doi:10.1016/j.toxlet.2010.03.1126
28. Wu X, Tan Y, Mao H, et al. Toxic effects of iron oxide nanoparticles on human umbilical vein endothelial cells. *Int J Nanomed*. 2010;5:385. doi:10.2147/IJN.S10458
29. Gholami L, Oskuee RK, Tafaghodi M, et al. Green facile synthesis of low-toxic superparamagnetic iron oxide nanoparticles (SPIONs) and their cytotoxicity effects toward Neuro2A and HUVEC cell lines. *Ceram Int*. 2018;44(8):9263–9268. doi:10.1016/j.ceramint.2018.02.137
30. Wang M, Shi GW, Bian CX, et al. UVA irradiation enhances brusatol-mediated inhibition of melanoma growth by downregulation of the Nrf2-mediated antioxidant response. *Oxid Med Cell Longev*. 2018;2018:9742154. doi:10.1155/2018/9742154
31. Xiang Y, Ye W, Huang C, et al. Brusatol enhances the chemotherapy efficacy of gemcitabine in pancreatic cancer via the Nrf2 signalling pathway. *Oxid Med Cell Longev*. 2018;2018(4b):1–10. doi:10.1155/2018/2360427
32. Wang J, Luo B, Li X, et al. Inhibition of cancer growth in vitro and in vivo by a novel ROS-modulating agent with ability to eliminate stem-like cancer cells. *Cell Death Dis*. 2017;8(6):e2887–e2887. doi:10.1038/cddis.2017.272
33. Wang J, Yi J. Cancer cell killing via ROS: to increase or decrease, that is the question. *Cancer Biol Ther*. 2008;7(12):1875–1884. doi:10.4161/cbt.7.12.7067
34. Piskounova E, Agathocleous M, Murphy MM, et al. Oxidative stress inhibits distant metastasis by human melanoma cells. *Nature*. 2015;527(7577):186–191. doi:10.1038/nature15726
35. Yu X, Lao Y, Teng XL, et al. SENP3 maintains the stability and function of regulatory T cells via BACH2 deSUMOylation. *Nat Commun*. 2018;9(1):3157. doi:10.1038/s41467-018-05676-6
36. Chen Y, Shen X, Han SL, et al. Irradiation pretreatment enhances the therapeutic efficacy of platelet-membrane-camouflaged antitumor nanoparticles. *J NanobiotechnoL*. 2020;18(1):1–11. doi:10.1186/s12951-020-00660-z
37. Gorrini C, Harris IS, Mak TW. Modulation of oxidative stress as an anticancer strategy. *Nat Rev Drug Discov*. 2013;12(12):931–947. doi:10.1038/nrd4002
38. Terasaki A, Kurokawa H, Indo HP, et al. Enhancement of PDT-cytotoxicity via ROS induced by indomethacin in metastatic breast cancer. *Porphyr Sci Women*. 2019;3:361–368.
39. Ming L, Cheng K, Chen Y, et al. Enhancement of tumor lethality of ROS in photodynamic therapy. *Cancer Med-US*. 2021;10(1):257–268. doi:10.1002/cam4.3592

40. Liu D, Zhang Y, Wei Y, et al. Activation of AKT pathway by Nrf2/PDGFA feedback loop contributes to HCC progression. *Oncotarget*. 2016;7(40):65389–65402. doi:10.18632/oncotarget.11700
41. Yang Y, Tian Z, Guo R, et al. Nrf2 inhibitor, brusatol in combination with trastuzumab exerts synergistic antitumor activity in HER2-positive cancers by inhibiting Nrf2/HO-1 and HER2-AKT/ERK1/2 pathways. *Oxid Med Cell Longev*. 2020;2020(6):1–14. doi:10.1155/2020/8825387
42. Lu Y, Wang B, Shi Q, et al. Brusatol inhibits HIF-1 signaling pathway and suppresses glucose uptake under hypoxic conditions in HCT116 cells. *Sci Rep-UK*. 2016;6(1):1–12.